# INTERNATIONAL SOCIETY FOR SOIL MECHANICS AND GEOTECHNICAL ENGINEERING



This paper was downloaded from the Online Library of the International Society for Soil Mechanics and Geotechnical Engineering (ISSMGE). The library is available here:

#### https://www.issmge.org/publications/online-library

This is an open-access database that archives thousands of papers published under the Auspices of the ISSMGE and maintained by the Innovation and Development Committee of ISSMGE.

The paper was published in the proceedings of the 20<sup>th</sup> International Conference on Soil Mechanics and Geotechnical Engineering and was edited by Mizanur Rahman and Mark Jaksa. The conference was held from May 1<sup>st</sup> to May 5<sup>th</sup> 2022 in Sydney, Australia.

## Applicability validation of energy-based liquefaction prediction method by comparison using a centrifugal model test

Validation de l'applicabilité de la méthode de prédiction de liquéfaction basée sur l'énergie par comparaison avec le test sur modèle centrifuge

#### Makoto Ishimaru & Masahiro Sawatsubashi

Sustainable System Research Laboratory, Central Research Institute of Electric Power Industry, Japan, ishimaru@criepi.denken.or.jp

ABSTRACT: In recent years, energy-based methods have attracted attention for rational liquefaction prediction. To verify the applicability of energy-based liquefaction prediction, its results were compared with those of stress-based prediction using a centrifugal model test. For the centrifugal model test, a saturated sand ground model with a relative density of 55% and height of 400 mm was made using silica sand and a viscous fluid, and seismic motion was input under a centrifugal acceleration of 25 G. In the test, the excess pore water pressure ratio reached unity only at part of the depth, but the stress-based liquefaction prediction method indicated a wide range of liquefaction. However, using the energy-based method, the depth at which the excess pore water pressure ratio was 0.95 or more matched with the test, and it was found that the energy-based method can reasonably predict liquefaction.

RÉSUMÉ: Ces dernières années, les méthodes basées sur l'énergie ont attiré l'attention en tant que méthodes de prédiction rationnelle de liquéfaction. Afin de vérifier l'applicabilité de la méthode de prédiction de liquéfaction basée sur l'énergie, les résultats d'un test de modèle centrifuge et les résultats de prédiction ont été comparés. Dans le test du modèle centrifuge, un modèle de sol de sable saturé avec une densité relative de 55% et une hauteur de 400 mm a été réalisé en utilisant du sable de silice et un fluide visqueux, et un mouvement sismique a été entré sous une accélération centrifuge de 25G. Dans le test, le rapport de pression d'eau interstitielle en excès n'a atteint 1 que sur une partie de la profondeur, mais la méthode FL (méthode de prédiction de liquéfaction basée sur les contraintes) a abouti à une liquéfaction à large plage. D'autre part, dans la méthode basée sur l'énergie, la profondeur à laquelle le rapport de pression d'eau interstitielle excédentaire était de 0,95 ou plus correspondait à l'essai, et il a été constaté que la méthode basée sur l'énergie peut raisonnablement prédire la liquéfaction.

KEYWORDS: sand, liquefaction prediction, dissipated energy, centrifugal model test, earthquake response analysis

#### 1 INTRODUCTION

Currently, in the liquefaction prediction of various standards, the "stress-based method," which predicts liquefaction by comparing the shear stress generated in the ground with the undrained cyclic shear strength, is used as standard. However, in the verification of liquefaction prediction for the damage cases of the 2011 Tohoku Earthquake off the Pacific coast of Japan, it was noted that the stress-based method is conservative.

Therefore, it is desirable to establish a more rational liquefaction prediction method, and in recent years, the "energy-based method" has attracted attention. The energy-based method compares the dissipated energy related to the occurrence of liquefaction and the energy on the supply side due to seismic motion in each ground layer (e.g., Berrill & Davis 1985, Kazama et al. 2000, Kokusho 2013, Ghorbani & Eslami 2021, Kokusho 2021). Because the dissipated energy is closely related to the increase in excess pore water pressure and decrease in shear rigidity, it can be expected to contribute to liquefaction prediction, including the degree of deformation. However, this method still has few application cases and has not been put into practical use.

The applicability of the energy-based method has been examined for liquefaction damage cases of past earthquakes (Kokusho & Mimori 2015), but the ground physical properties and input waves may be unclear in actual disaster cases. Therefore, in this study, we analyzed the characteristics of the energy-based method in comparison to those of the stress-based method, especially from the viewpoint of predicting the increase in excess pore water pressure using a centrifugal model test with saturated sand.

#### 2 TEST CONDITIONS

Figure 1 shows an illustration of the ground model and the arrangement of the measuring instruments. The ground model used in this study was created with a 1/25 reduction ratio, and seismic motion was input in a centrifugal force field with a centrifugal acceleration of 25 G. Table 1 lists the specifications of the centrifugal model test according to similarity laws (e.g., Kazama & Inatomi 1993).

Table 1. Specifications of the centrifugal model test according to similarity laws

Similarity laws.		
Parameter	Real	Model
Length	1	1/25
Strain	1	1
Stress	1	1
Time	1	1/25
Displacement	1	1/25
Velocity	1	1
Acceleration	1	25

#### 2.1 Ground model and measurement items

The ground model was prepared using silica sand No. 7 and a viscous fluid (aqueous solution of methyl cellulose adjusted to  $25 \text{ mN/m}^2 \cdot \text{s}$ ) in a shear soil tank. The ground height was 400 mm

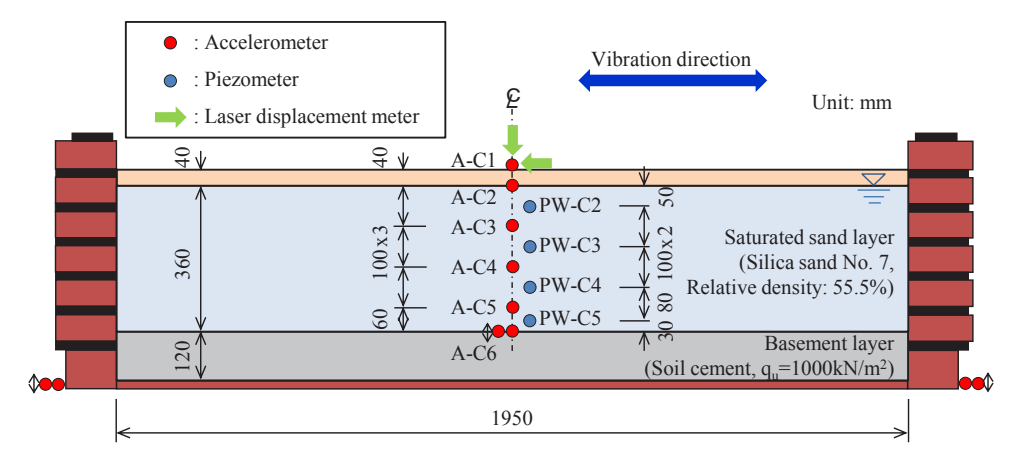


Figure 1. Ground model and arrangement of the measuring instruments.

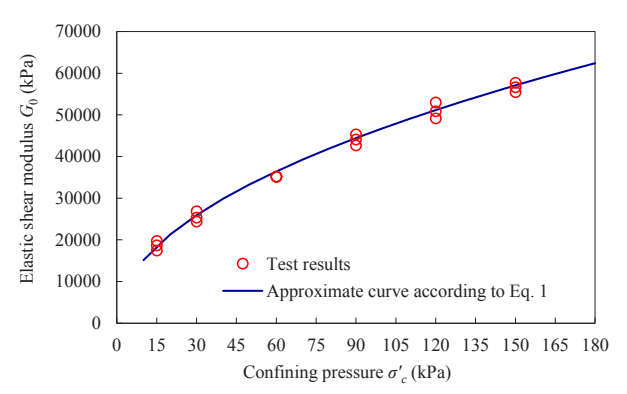


Figure 2. Elastic shear modulus test results (red circles) and approximate curve according to Eq. 1 (blue curve).

(10 m at real scale), and the groundwater level was -40 mm (-1 m at real scale) from the ground surface.

The method used to produce the ground model was as follows. A liquefied (saturated) layer was prepared by dropping the sand into a degassed viscous fluid, and then the surface ground above the groundwater level was prepared by dropping the sand in the air. The relative density was 55.5% for the liquefied layer and 69.0% for the non-liquefied layer. The measurement items were acceleration, displacement of the ground surface, and underground water pressure.

#### 2.2 Physical properties of geomaterial

The basic physical properties of silica sand No. 7 are a soil particle density of 2.625 Mg/m³, maximum void ratio of 1.198, and minimum void ratio of 0.699. The shear modulus, dynamic deformation characteristics, and liquefaction strength were determined by cyclic triaxial tests using specimens (diameter 50 mm × height 100 mm) with a relative density of approximately 55%.

#### 2.2.1 Elastic shear modulus

Regarding elastic shear modulus, minute cyclic loadings were performed under various confining pressure conditions, and the relationship between the confining pressure  $\sigma_c'$  (kPa) and elastic shear modulus  $G_0$  (kPa) was determined. Figure 2 shows the test results and approximate curve according to Eq. 1.

$$G_0 = 4900 \cdot \sigma_c^{\prime 0.49} \tag{1}$$

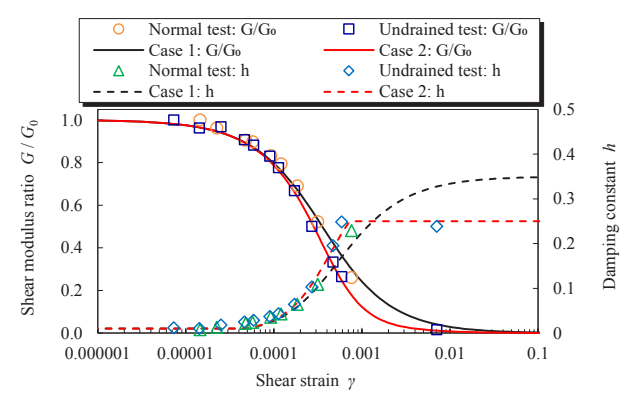


Figure 3. Dynamic deformation characteristics obtained from the cyclic triaxial tests (confining pressure: 30 kPa).

### 2.2.2 Dynamic deformation characteristics

Figure 3 shows the dynamic deformation characteristics obtained from cyclic triaxial tests. The cyclic triaxial tests were performed at confining pressures of 30 and 60 kPa, but no effect was observed from the confining pressure. Note that "Normal test" refers to the test conducted according to the test standard (Japanese Geotechnical Society 2000), and "Undrained test" refers to the test under the condition that no drainage was performed between the loading steps assuming liquefaction. In the figure, the test results are fitted with the general hyperbolic equation (GHE) model (Tatsuoka & Shibuya 1992), as formulated in Eq. 2.

$$G/G_0 = \frac{1}{\frac{1}{C_1(\gamma)} + \frac{1}{C_2(\gamma)} \cdot \frac{\gamma}{\gamma_r}}$$
(2)

where  $\gamma$  is shear strain, G is shear modulus, and  $\gamma_r$  is the reference shear strain.  $C_1(\gamma)$  and  $C_2(\gamma)$  are correction coefficients defined as follows:

$$C_{1}(\gamma) = \frac{C_{1}(0) + C_{1}(\infty)}{2} + \frac{C_{1}(0) - C_{1}(\infty)}{2} \cdot \cos\left\{\frac{\pi}{\alpha/(|\gamma|/\gamma_{r}) + 1}\right\}$$
(3a)

$$C_2(\gamma) = \frac{C_2(0) + C_2(\infty)}{2} + \tag{3b}$$

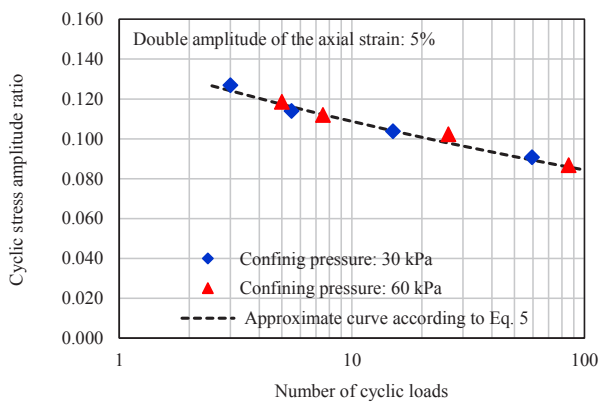


Figure 4. Relationship between the number of cyclic loads and the cyclic stress amplitude ratio in liquefaction tests.

$$\frac{C_2(0)-C_2(\infty)}{2}\cdot\cos\left\{\frac{\pi}{\beta/(|\gamma|/\gamma_r)+1}\right\}$$

where  $C_1(0)$ ,  $C_2(0)$ ,  $C_1(\infty)$ ,  $C_2(\infty)$ ,  $\alpha$ , and  $\beta$  are parameters. The damping characteristics are assumed to follow the model given in Eq. 4.

$$h = h_{max} \cdot (1 - G/G_0)^{\beta_1} \tag{4}$$

where  $h_{max}$  is the maximum damping constant, and  $\beta_1$  is the adjustment parameter for the damping characteristics.

The parameter settings of the GHE model are listed in Table 2. The lower limit of the damping constant was 0.01, and the damping constant for Case 2 was set to 0.25, which is the upper limit based on the test results. It was confirmed that in Case 2, the shear modulus ratio decreased faster and the damping constant increased faster than in Case 1.

Table 2. Parameter settings of the GHE model.

Parameter	Case 1	Case 2
1 drameter	(Normal test)	(Undrained test)
$C_{1}(0)$	1.00	1.00
$\mathcal{C}_1(\infty)$	1.00	1.00
$C_{2}(0)$	1.00	1.00
$C_2(\infty)$	0.75	0.20
α	1.00	1.00
β	1.00	1.00
$\gamma_r$	0.0004	0.0004
$h_{min}$	0.01	0.01
$h_{max}$	0.35	0.35
$eta_1$	1.60	1.60

#### 2.2.3 Liquefaction strength

Figure 4 shows the relationship between the number of cyclic loads  $N_C$  and the cyclic stress amplitude ratio CSR when the double amplitude of the axial strain DA was 5% for the liquefaction strength test. From the figure, it can be confirmed that there was no difference owing to the confining pressure. When the power approximation was performed using the least squares method, the following relationship was obtained:

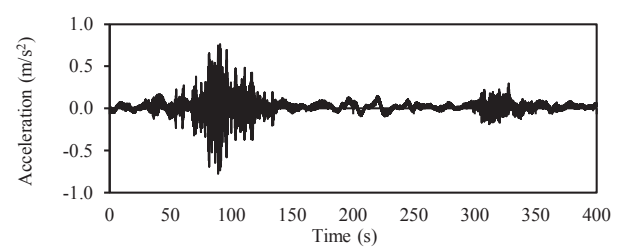


Figure 5. Horizontal acceleration at the upper surface of the basement layer (A-C6).

$$CSR = 0.14 \cdot N_C^{-0.11} \tag{5}$$

Thus, the liquefaction strength  $R_L$  (CSR with  $N_c = 20$ ) was 0.10.

#### 2.3 Input seismic motion

The input seismic motion was created by pulling back the observed waves of K-NET Urayasu from the 2011 Tohoku Earthquake off the Pacific coast to the lower part of the liquefaction layer by one-dimensional seismic response analysis using the ground model of the observation site. In the input of the test, the acceleration amplitude of the pulled back seismic motion and interval between the mainshock and aftershock were adjusted. Figure 5 shows the horizontal acceleration at the upper surface of the basement layer (absolute maximum: 0.77 m/s²). In addition, all data after this are shown as values converted to the real scale based on Table 1.

#### 3 TEST RESULTS

Figures 6 and 7 show the excess pore water pressure ratio  $\Delta u/\sigma'_v$  (obtained by dividing the excess pore water pressure  $\Delta u$  by the initial vertical effective stress  $\sigma'_v$ ) at each depth and the vertical displacement of the ground surface, respectively. From Fig. 6,  $\Delta u/\sigma'_v$  of PW-C3 reached one, and it is presumed that liquefaction occurred in this layer.

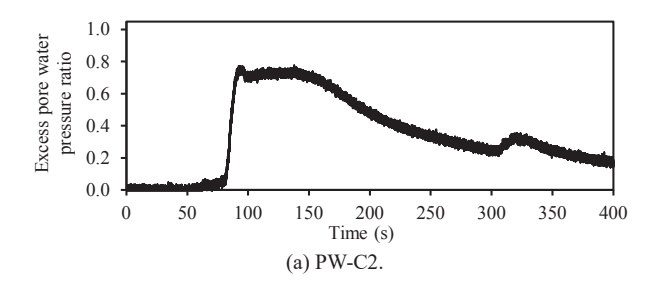
However, the vertical displacement of the ground surface had a residual displacement of approximately 58 mm, but most of this occurred during excitation, and the ratio of displacement owing to excess pore water pressure dissipation after excitation was small. In addition, the horizontal acceleration in the ground tended to increase from the upper surface of the basement layer to the ground surface.

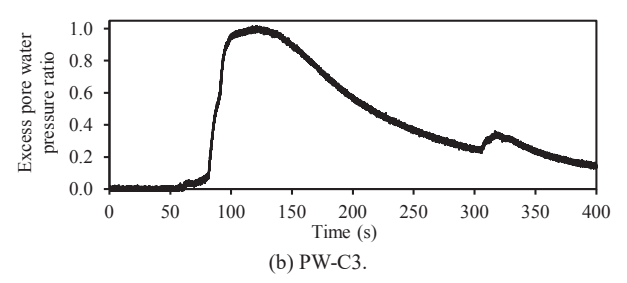
#### 4 APPLICABILITY OF LIQUEFACTION PREDICTION

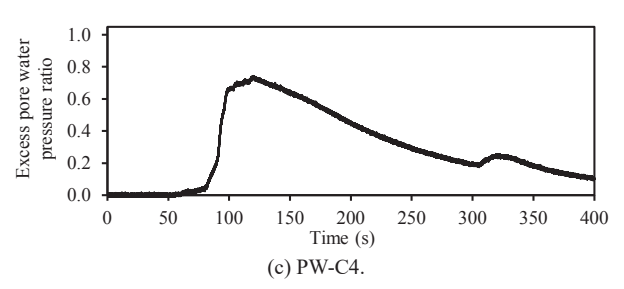
In this study, we first performed one-dimensional equivalent linear analyses using the horizontal acceleration at the upper surface of the basement layer, as shown in Fig. 5.

#### 4.1 Equivalent linear analysis

Table 3 summarizes the physical characteristics in the analysis. The ground was divided into intervals of 1-m layer thickness. The elastic shear modulus was set using Eq. 1 by assuming a coefficient of earth pressure at rest of 0.5 and calculating the mean effective stress. For the dynamic deformation characteristics, two sets of values, those of Cases 1 and 2, were used, as shown in Fig. 3 and Table 2. In addition, the effective strain coefficient in the equivalent linear analyses was set to 0.65.







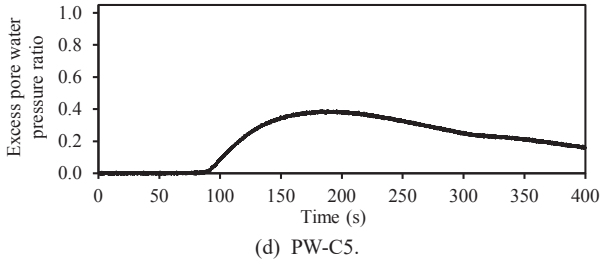


Figure 6. Excess pore water pressure ratio at each depth.

Table 3. Physical characteristics in the analysis

Table 3. Physical characteristics in the analysis.					
	Layer		Initial	Initial	Elastic
	center	Wet	effective	effective	shear
Layer	depth	density	vertical	mean	modulus
			stress	stress	
	(m)	$(Mg/m^3)$	$(kN/m^2)$	$(kN/m^2)$	$(kN/m^2)$
1	0.5	1.415	6.94	4.63	10378.2
2	1.5	1.845	18.02	12.01	16566.4
3	2.5	1.845	26.31	17.54	19940.7
4	3.5	1.845	34.59	23.06	22804.2
5	4.5	1.845	42.88	28.59	25334.6
6	5.5	1.845	51.17	34.11	27625.7
7	6.5	1.845	59.45	39.64	29734.2
8	7.5	1.845	67.74	45.16	31697.4
8	1.3	1.043	07.74	45.10	31097.4
9	8.5	1.845	76.03	50.68	33541.5
10	9.5	1.845	84.31	56.21	35285.7

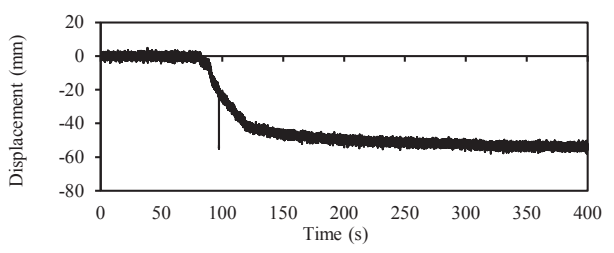


Figure 7. Vertical displacement of the ground surface.

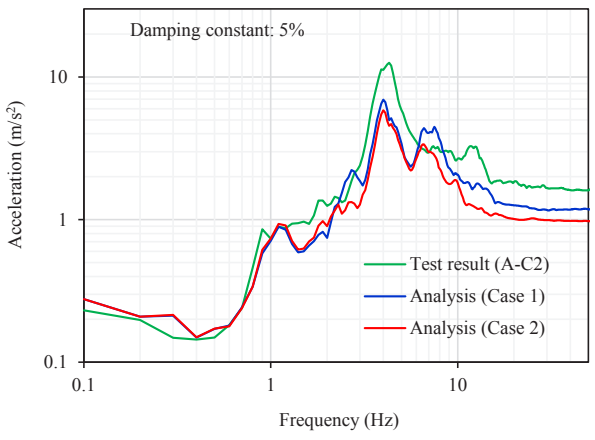


Figure 8. Response spectra of the horizontal acceleration at -1 m from the ground surface.

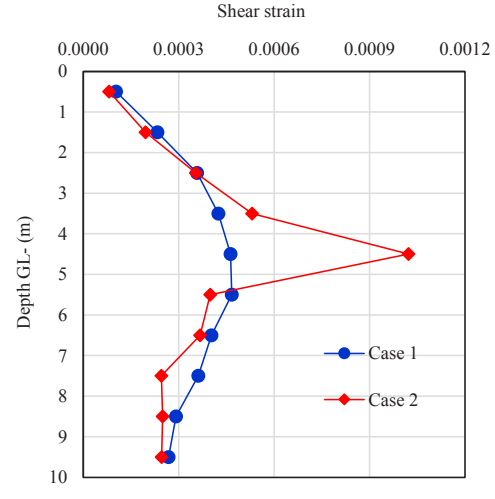


Figure 9. Depth distributions of the maximum values of shear strain in the equivalent linear analyses.

Figure 8 shows the response spectra of the horizontal acceleration at -1 m from the ground surface (groundwater level position) in comparison with that of the test result (A-C2). From this figure, it is considered that the acceleration response of the test result can be reproduced relatively well, even in the equivalent linear analyses.

Figure 9 shows the depth distributions of the maximum shear strain values in the equivalent linear analyses. From this, it can be confirmed that the shear strain tended to increase near the 5th layer in both cases, but in Case 2, the non-linearity of the 5th layer was particularly notable. As shown in Fig. 3, the shear modulus under non-drainage conditions dropped sharply at a relatively large strain level, so it is considered that in Case 2, the deformation was further concentrated in the 5th layer, which originally had a large shear strain.

#### 4.2 Liquefaction prediction by stress-based method

In the stress-based method, it is judged that there is a possibility of liquefaction when  $F_L$  (= R/L)  $\leq$  1. Here, R is the dynamic shear strength ratio, and L is the shear stress ratio during an earthquake. The dynamic shear strength ratio was set to  $R = R_L$ = 0.10 in this study. The shear stress ratio during an earthquake was calculated by dividing the maximum value of the shear stress of each layer in the equivalent linear analyses by the initial vertical effective stress  $\sigma_{\nu}'$ .

Table 4 lists the results of liquefaction prediction using the stress-based method. From this, it can be confirmed that liquefaction occurred in a wide range from below the groundwater level to approximately GL-6 to 7 m, regardless of which of the equivalent linear analysis results of Cases 1 and 2 was used. In the test, the excess pore water pressure ratio  $\Delta u/\sigma_{\nu}'$ near GL-5 m was larger than that near GL-3 m, but this tendency was not observed from the value of  $F_L$ . Comparing Cases 1 and 2, it can be said that Case 1 is a conservative evaluation because the value of  $F_L$  is smaller and the range below one is wider.

Table 4. Results of liquefaction prediction by the stress-based method.

		merane in p		ne berebb cub	
Layer	Absolute maximum value of shear stress (kN/m²)		Excess pore water pressure ratio	$F_L$	
	Case 1	Case 2	Test	Case 1	Case 2
1	0.92	0.73	_	_	_
2	2.81	2.31	_	0.65	0.79
3	4.49	3.92	0.78	0.59	0.68
4	5.57	5.11	_	0.63	0.68
5	6.53	5.77	1.02	0.66	0.75
6	6.86	5.60	-	0.75	0.92
7	6.84	5.28	_	0.88	1.13
8	6.77	5.49	0.74	1.01	1.24
9	6.42	5.85	_	1.19	1.31
10	6.79	6.21	0.39	1.25	1.37

#### Liquefaction prediction by energy-based method

#### 4.3.1 Dissipated energy of sand

Regarding the liquefaction strength tests shown in Fig. 4, the relationships between the excess pore water pressure ratio  $\Delta u/\sigma_c'$  and normalized accumulated dissipated energy  $\sum \Delta W / \sigma_c'$  are shown in Fig. 10 for each confining pressure.  $\sum \Delta W/\sigma_c'$  was calculated by the following equation:

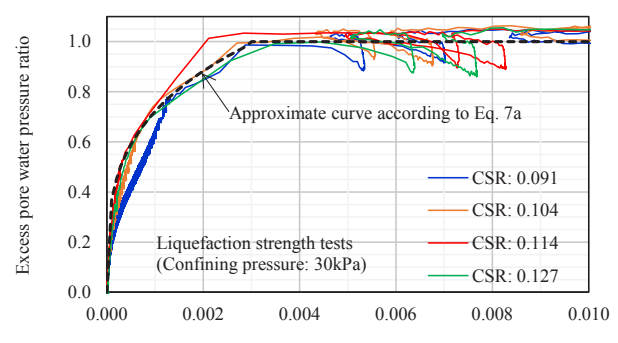
$$\sum \Delta W / \sigma_c' = \oint \tau(\gamma) d\gamma / \sigma_c' = \int_0^t \tau(\gamma) \dot{\gamma}(t) dt / \sigma_c'$$
 (6)

where  $\tau$  is shear stress. From Fig. 10, as in previous studies (e.g., Kazama et al. 2000, Kokusho 2013), a unique relationship was found between the increase in  $\Delta u/\sigma_c'$  and  $\sum \Delta W/\sigma_c'$ . Figure 10 also shows the following curves, which approximate the upper limit of the test results.

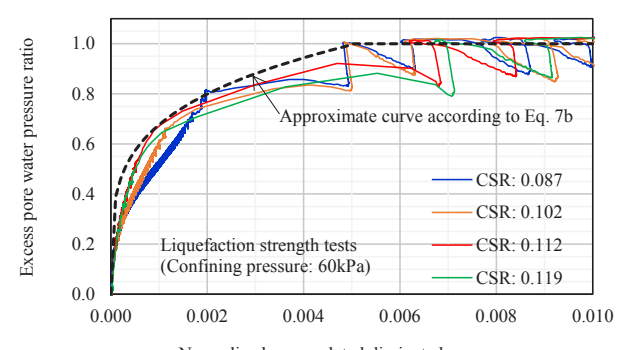
Confining pressure of 30 kPa:

$$\Delta u/\sigma_c' = 5.35 \cdot (\sum \Delta W/\sigma_c')^{0.29} \ (\sum \Delta W/\sigma_c' < 0.003)$$
  
$$\Delta u/\sigma_c' = 1.00 \ (\sum \Delta W/\sigma_c' \ge 0.003)$$
 (7a)

Confining pressure of 60 kPa:



Normalized accumulated dissipated energy (a) Confining pressure: 30 kPa.



Normalized accumulated dissipated energy

(b) Confining pressure: 60 kPa.

Figure 10. Relationships between the excess pore water pressure ratio and normalized accumulated dissipated energy obtained from liquefaction strength tests.

$$\Delta u/\sigma'_c = 3.55 \cdot (\sum \Delta W/\sigma'_c)^{0.24} (\sum \Delta W/\sigma'_c < 0.005)$$
 (7b)  
 $\Delta u/\sigma'_c = 1.00 (\sum \Delta W/\sigma'_c \ge 0.005)$ 

In addition, it was confirmed that the value of  $\sum \Delta W/\sigma'_c$  at which the excess pore water pressure ratio is 0.95 or more is approximately 0.003 at a confining pressure of 30 kPa.

#### Dissipated energy due to seismic motion

The normalized accumulated dissipated energy due to seismic motion was calculated using the method described by Kazama et al. (2000) as follows:

1) Using the equivalent linear analysis results, the time history of the elastic strain energy  $W_E$  for each ground layer was calculated by the following equation:

$$W_E(t) = G_{eq} \cdot \{\gamma(t)\}^2 / 2 \tag{8}$$

where  $G_{eq}$  is the convergence value of the shear modulus. 2) From the maximum value  $W_{E,i}^{pk}$  of the i-th pulse in the time history of  $W_E$ , the dissipated energy  $\Delta W_i$  was calculated for each pulse by the following equation:

$$\Delta W_i = 4\pi \cdot h_{eq} \cdot W_{E,i}^{pk} / 2 \tag{9}$$

where  $h_{eq}$  is the convergence value of the damping constant. In addition, because each pulse corresponds to half-cycle loading-unloading, it was divided by 2 to obtain a half-cycle 3) The normalized accumulated dissipated energy was calculated by accumulating  $\Delta W_i$  in Eq. 9 and dividing by the initial vertical effective stress  $\sigma'_{\nu}$ .

#### 4.3.3 Results of liquefaction prediction

Table 5 lists the normalized accumulated dissipated energies due to the seismic motion for Cases 1 and 2. Table 5 also lists the excess pore water pressure ratios calculated by Eq. 7a. In addition, because the normalized accumulated dissipated energy at a depth with a large confining pressure was small and did not affect the prediction result, only the approximate curve with a confining pressure of 30 kPa was used for calculating the excess pore water pressure ratios. From this table for Case 1, it can be confirmed that there was no layer of 0.95 or more, although the excess pore water pressure ratios around GL-4 to 5 m were large. For Case 2, the layer where the excess pore water pressure ratio reached one in the test was 0.95 or more, and it can be said that the occurrence of liquefaction in the test can be reproduced relatively well.

Table 5. Results of liquefaction prediction by the energy-based method.

	Norm	alized			
Layer	accumulated		Excess pore water pressure ratio		
	dissipated energy				
	Case 1	Case 2	Test	Case 1	Case 2
1	-	_	_	_	_
2	0.0003	0.0002	_	0.51	0.45
3	0.0008	0.0007	0.78	0.68	0.65
4	0.0010	0.0014	_	0.72	0.80
5	0.0010	0.0033	1.02	0.72	1.00
6	0.0008	0.0005	_	0.68	0.59
7	0.0005	0.0004	_	0.59	0.55
8	0.0004	0.0002	0.74	0.55	0.45
9	0.0002	0.0002	_	0.45	0.45
10	0.0002	0.0002	0.39	0.45	0.45

Figure 11 shows the normalized accumulated dissipated energy calculated from the equivalent linear analysis results for the 5th layer of Case 2 and the excess pore water pressure ratio (PW-C3) of the test. From this figure, it can be confirmed that the time when the normalized accumulated dissipated energy reached approximately 0.003 and the time when the excess pore water pressure ratio reached one were almost the same, and the increase in excess pore water pressure can be predicted accurately by the energy-based method.

#### 5 CONCLUSIONS

In this study, we investigated the applicability of two types of liquefaction prediction methods for a centrifugal model test with saturated sand: stress-based and energy-based. The findings of this study can be summarized as follows:

- The test results show that the excess pore water pressure ratio reached one only at part of the depth, but the stress-based method indicated liquefaction over a wide area.
- Using the energy-based method, the depth at which the excess pore water pressure ratio was 0.95 or more agreed with the test results, and it was confirmed that liquefaction can be reasonably predicted by the energy-based method.
- For the equivalent linear analysis used in the energy-based method, it was confirmed that the prediction accuracy is better

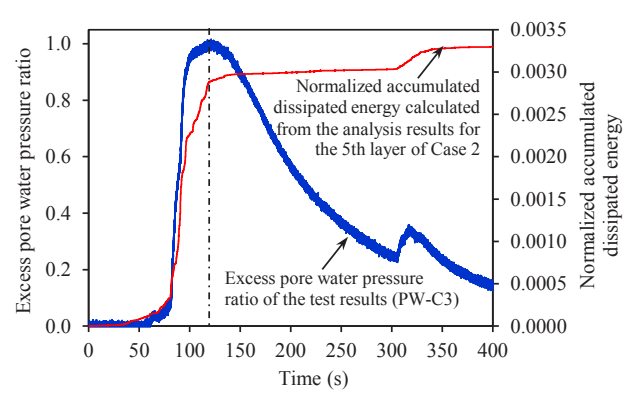


Figure 11. Normalized accumulated dissipated energy calculated from the equivalent linear analysis results for the 5th layer of Case 2 and the excess pore water pressure ratio (PW-C3) of the test.

if dynamic deformation characteristics that consider the effects of non-drainage conditions (i.e., liquefaction) are used. In the future, we plan to study cases with different ground conditions and input conditions and contribute to the practical application of liquefaction prediction by the energy-based method.

#### 6 ACKNOWLEDGEMENTS

We used the strong motion record of NIED K-NET, KiK-net (National Research Institute for Earth Science and Disaster Resilience, doi:10.17598/NIED.0004).

#### 7 REFERENCES

Berrill, J. B. and Davis, R. O. 1985. Energy dissipation and seismic liquefaction of sands: revised model. *Soils and Foundations* 25 (2), 106–118

Ghorbani, A. and Eslami, A. 2021. Energy-based model for predicting liquefaction potential of sandy soils using evolutionary polynomial regression method. *Computers and Geotechnics* 129, https://doi.org/10.1016/j.compgeo.2020.103867.

Japanese Geotechnical Society. 2000. JGS 0542 Method for cyclic triaxial test to determine deformation properties of geomaterials. Laboratory Testing Standards of Geomaterials 2.

Kazama, M. and Inatomi, T. 1993. Application of centrifuge model testing to dynamic problems. *Proceedings of JSCE* (477), 83–92 (in Japanese).

Kazama, M., Yamaguchi, A. and Yanagisawa, E. 2000. Liquefaction resistance from a ductility viewpoint. Soils and Foundations 40 (6), 47–60

Kokusho, T. 2013. Liquefaction potential evaluations: energy-based method versus stress-based method. *Canadian Geotechnical Journal* 50 (10), https://doi.org/10.1139/cgj-2012-0456.

Kokusho, T. and Mimori, Y. 2015. Liquefaction potential evaluations by energy-based method and stress-based method for various ground motions. Soil Dynamics and Earthquake Engineering 75, 130–146.

Kokusho, T. 2021. Energy-based liquefaction evaluation for induced strain and surface settlement - evaluation steps and case studies -. Soil Dynamics and Earthquake Engineering 143, https://doi.org/10.1016/j.soildyn.2020.106552.

Tatsuoka, F. and Shibuya, S. 1992. Deformation characteristics of soils and rocks from field and laboratory tests. *Proc. 9th Asian Regional Conf. Soil Mechanics and Foundation Engineering*, Bangkok, Thailand, 2, 101–170.